CHAPTER III

RESULTS AND DISCUSSION

Catalyst Characterization

The results for all methods of preparation are given in this section. The effect of calcination time, temperature, and method of preparation on catalyst properties will be discussed first. A separate sub-section discussing the catalysts prepared for the oxygen vacancy experiments is included because these catalysts should be compared in context with each other.

Effect of calcination time, temperature, and method of preparation

A batch of precipitated zirconia was prepared to examine the effect of calcination time on the surface area and structure. This batch was divided into smaller samples after the drying step. Each sample was placed in the muffle furnace after the temperature had reached 773 K. Table 3.1 shows the changes in surface area and XRD pattern with time.

The distinction between crystal phases was made based on the interlayer spacing (d spacing) and relative intensities found in XRD analysis. The d spacing and relative intensities for each of the polymorphs of zirconia are shown in Table 3.2.

The XRD patterns for the samples in Table 3.1 are shown in Figures 3.1, 3.2, and 3.3 respectively. In all XRD patterns the bottom axis is the diffraction angle (2θ) in degrees, the top axis is d spacing (Å), and the left axis is intensity. The numbers printed by the major peaks are d spacing and intensity for that peak. With increasing calcination time at 773 K, more of the sample is converted from the cubic phase to the monoclinic phase. When an equal mixture of samples calcined for 5, 30, and 180 minutes were recalcined for 3½ hours (again with furnace hot) a mixture of monoclinic and cubic zirconia resulted with a surface area of 48 m^2/g. The sample was recalcined again for 3 hours and no change in XRD pattern was observed and the surface area decreased slightly to 47 m^2/g.

A larger batch of precipitated zirconia was also prepared to observe how surface area and structure changed with higher calcination temperatures. The entire batch was subjected to drying at 383 K for 24 hours. After this, the batch was divided into three samples. These results are shown in Table 3.3.

The XRD patterns for these samples are shown in Figures 3.4, 3.5, and 3.6 respectively. The sample calcined at 1273 K resulted in a completely monoclinic zirconia. Calcination at 723 K gave a mixture of cubic and monoclinic phases. Calcining at 773 K gave predominantly monoclinic zirconia when the normal calcination procedure was followed, while calcining at 723 K resulted in predominantly cubic. The samples that were calcined at 773 K also did not spend as much time in the mother liquor (as gel) before they were filtered and washed. This may also contribute to the stabilization of the cubic phase.

Figure 3.7 shows a predominantly monoclinic zirconia obtained by calcining at 773 K, while Figure 3.5 shows the result at 723 K. Normally, the cubic phase is not stable at room temperature, but this is only after high temperature (>1000 K) calcination. These high temperatures are used to sinter the zirconia for use as a structural ceramic. In this study, 723 K calcination was used in the majority of precipitated samples. This temperature

gave higher surface areas than those obtained at 773 K and was greater than or equal to the maximum reaction temperature. Fully stabilized cubic zirconia could be prepared by the addition of dopant cations of larger size or lower charge than zirconium. More explanation of this stabilization is given in the section on oxygen vacancy catalysts. Figure 3.8 shows the XRD pattern of a fully stabilized cubic zirconia doped with cerium.

The first hydrothermal preparation resulted in the cubic phase while the second resulted in a mixture of cubic and monoclinic. The XRD pattern for the first preparation is shown in Figure 3.9. The decreased cooking time and lesser amount of stabilizing cations in the second sample may be the reason the cubic phase was not fully stabilized. Both of these samples were calcined at 773 K.

Preparation of zirconia by calcining zirconyl nitrate resulted in a mixture of the cubic and monoclinic phases as seen in Figure 3.10. A drawback to this preparation method is that dopants cannot be added to the zirconia without calcining at much higher temperatures.

Preparation by the modified sol gel method resulted in mainly tetragonal zirconia as shown in Figure 3.11. The commercial zirconia catalyst (Harshaw H-0304) was monoclinic. Doping the catalyst with alkali or alkaline earth metals usually stabilized the cubic phase depending on the level of doping. More discussion on this subject will be given in the section on oxygen vacancy catalysts.

The pore volume, pore diameter, and bulk density varied with preparation method. Typical values obtained for these quantities using the different preparation methods are shown in Table 3.4. The pore size distribution of both precipitated and hydrothermal catalysts is unimodal. Precipitated catalysts had pore diameters of 30-40 Å while the hydrothermal catalysts had pore diameters of 150-200 Å. Calcining zirconyl nitrate resulted in a zirconia with properties of both the precipitated and hydrothermal samples. The pore size distribution was bimodal with pores in both the 30-40 Å and 150-200 Å ranges. The bulk density of these catalysts increased in the order hydrothermal < calcining < precipitated while pore volumes decreased in the same order.

The results of preparations for all catalysts, including those for oxygen vacancy experiments, used for isobutylene synthesis are presented in Table 3.5.

Modification of acid-base properties

The impact of acid-base properties on isosynthesis activity has been suggested in previous studies (*14,15,38*). By definition, an acid is a proton donor (Brönsted acid) or electron acceptor (Lewis acid), and a base is a proton acceptor (Brönsted base) or electron donor (Lewis base). Zirconia is bifunctional with both acid and base properties:

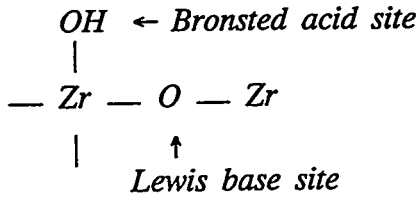

Changes in the preparation procedure often results in a final material with different acidity and basicity (*38*). The acid-base properties can also be modified by adding other metal oxides with cations of varying size and valence (*15*). This section discusses the modification of the acid-base properties of zirconia by changing preparation method (commercial vs.

modified sol gel) and by doping the zirconia with other metal oxides. In the discussion on doping, catalysts doped with alumina and silica will be presented first, followed by those doped with oxides of alkali and alkaline earth metals. These catalysts were prepared by the modified sol gel method.

The commercial zirconia (obtained from Harshaw) was prepared by calcination of zirconyl salts at temperatures over 873 K (*39,40*). It is referred to as ZrO_2 (H-0304). This commercial zirconia has been used previously for isosynthesis (*41*). Zirconia prepared by the modified sol gel method using an organic base $(CH_3)_4NOH$ is referred to as ZrO_2 (MSG). Figure 3.12 compares the basicity of ZrO_2 (MSG) and ZrO_2 (H-0304) as measured by temperature programmed desorption of CO_2. Surface area is not a contributing factor in these measurements since the difference in surface areas is less than 10%. Both catalysts show multiple adsorption sites with similar distribution of weak and strong sites, but ZrO_2 (MSG) has a larger number of basic sites than ZrO_2 (H-0304). The distributions of acidic sites, on the other hand, are fairly close over the two catalysts (Figure 3.13).

Both the total number and the distribution of sites are changed when aluminum or silicon are added to zirconium oxide (Figures 3.14 and 3.15). When aluminum is present with zirconia, stronger acidic sites are formed on the surface:

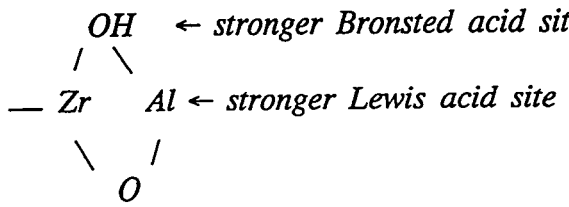

Basicity is also enhanced since electrons are donated by aluminum and are attracted to the electronegative surface oxygen ions making the oxygen ions more basic (*42*). On the other hand, when silicon is added to zirconia, basicity decreases whereas acidity increases, as also shown in Figures 3.14 and 3.15. The mole ratio of Al to Zr is 0.28 on the surface as measure by XPS, whereas the ratio is 0.17 in the bulk as measured by AA.

The effect of adding alkali metal (lithium, sodium, potassium, rubidium and cesium) on modified sol gel isosynthesis catalyst was studied. Doping with alkali metal modifies the acid-base properties, as shown in Figures 3.16 and 3.17. The distribution of metal in the catalysts is not the same for all the alkali-promoted zirconias. The mole ratio of Na to Zr on the surface is about 0.20, whereas the ratio in the bulk is 0.042. On the other hand, the mole ratio of K to Zr is 0.045 on the surface and 0.017 in the bulk.

The effect of adding alkaline earth metals (magnesium, calcium and barium) on isosynthesis catalyst was also studied. Doping with alkaline metal modifies the acid-base properties, as shown in Figures 3.18 and 3.19.

Catalysts used in oxygen vacancy experiments

Table 3.6 gives the ionic radii (*43*) of the dopants used in this study as well as those of some other cations used in ionic conductivity studies.

Lithium, magnesium, dysprosium, and tantalum were chosen as the +1, +2, +3, and +5 dopants respectively because their ionic radii were fairly close to that of zirconium (~15% different). Additionally, dysprosia was shown to be active for isosynthesis by Kieffer *et al.* (*8*). Aluminum was also used as a dopant even though cubic zirconia can only

dissolve ≈1 mol% of α-Al_2O_3 (*44*) (may be slightly higher for precipitation method) because Rajendran *et al.* (*45,46*) reported that addition of alumina to cubic stabilized zirconia reduces the grain boundary resistivity and increases the overall ionic conductivity. Also, the amount of aluminum that was incorporated into the lattice could be used to test the smaller ion → higher conductivity theory. The yttrium-barium-copper doped zirconia was synthesized because the compound $YBa_2Cu_3O_{7-x}$ (also called the '123' superconductor) was the first high temperature superconductor and is known to have oxygen vacancies. Since the superconductivity is associated with oxygen vacancies, the possibility of increased vacancy mobility (and thus catalyst activity) while maintaining the isosynthesis product distribution motivated the investigation of this catalyst. The equation for this series of dopants (shown below) is similar to the others except that two of the cations are +2 and one is +3.

$$Y_2O_3 + 4BaO + 6CuO \xrightarrow{12ZrO_2} 2Y_{Zr}' + 4Ba_{Zr}'' + 6Cu_{Zr}'' + 13O_O + 11V_O^{\bullet\bullet}$$

The results of the catalyst preparations (batch numbers 9-22 and 24) are shown in Table 3.5. Silver *et al.* (*47*) have shown that bulk (by atomic absorption) and surface (by X-ray photoelectron spectroscopy) dopant concentrations of precipitated zirconia are nearly identical. The XRD patterns of both the lithium and magnesium doped zirconias all showed some trace of the monoclinic phase. The trace was slightly stronger in the case of magnesium. The cubic phase is stabilized both by larger cations (as compared to zirconium) and oxygen vacancies. Doping with lithium and magnesium introduces oxygen vacancies because of their lower valences.

However, as shown in Table 3.6, the ionic radii of lithium and magnesium cations are smaller than that of zirconium. The cubic zirconia is stabilized by the vacancies and destabilized by the smaller cation. The monoclinic fraction of the magnesium doped zirconias may have been slightly larger because the magnesium cation is slightly smaller than the lithium cation and more oxygen vacancies are introduced per lithium cation than for magnesium. The aluminum doped zirconias were fully stabilized in the cubic form. This is a result of the creation of oxygen vacancies and smaller grain (crystal) size (*45,46*). A comparison between the XRD patterns of two alumina doped catalysts showed that the more heavily doped zirconia had broader, less intense peaks.

This is also characteristic of a finer grain (crystal) size, which is a result of adding alumina (*45,46*). No α-Al_2O_3 could be detected in either pattern. The dysprosium doped catalysts had the XRD patterns of fully stabilized cubic zirconia. This was expected because the dysprosium cation introduces oxygen vacancies and is larger than the zirconium cation. The XRD pattern for the Ta/Zr=0.04 catalyst showed the catalyst had more monoclinic character than the pure zirconia sample. This is a result of oxygen vacancies being eliminated (zirconium vacancies being created). When oxygen vacancies are eliminated the zirconium cation cannot support eightfold coordination with oxygen ions. Thus it becomes 7 coordinated and the monoclinic phase forms. A second compound was not detected in this pattern. The monoclinic peaks were predominant (more zirconium vacancies created) in the Ta/Zr=0.24 catalyst. Also, the primary peak for Ta_2O_5 was present. The '123' catalyst was cubic for the same reasons as the dysprosium catalyst.

The surface areas were all fairly high (85-130 m^2/g) except for the tantalum doped catalyst. This may be the result of more of the monoclinic phase being present in these samples. The higher surface areas of the alumina doped catalyst was most likely the result of small quantities of a separate high surface area alumina phase being formed. As

mentioned previously, cubic zirconia can only dissolve $\approx$1 mol% of α-Al_2O_3. The loss in surface area after reaction will be discussed in the next section. All catalysts used in the oxygen vacancy experiments were subjected to reaction conditions for ~26 hours.

The bulk densities for the pure, lithium doped, and magnesium doped zirconias were statistically the same ($\approx$2.16 g/cm^3). This is expected even though the molecular weights of lithium and magnesium are small compared to zirconium because the dopant is present in low concentrations. The aluminum doped catalysts had slightly lower bulk densities. This is probably the result of the less dense α-Al_2O_3 phase being present. A higher level of alumina doping led to a further decrease in bulk density. The dysprosium samples had higher densities because the much heavier dysprosium ion was substituted for zirconium. The tantalum catalysts had lower bulk densities because more of the less dense monoclinic phase was present and zirconium was being rejected from the lattice. The '123' zirconia had a slightly higher bulk density because of the incorporated barium.

Table 3.7 shows the number and type of defects introduced into the zirconia lattice for each dopant. Catalysts were prepared in order to test activity at constant vacancy to zirconium ratio (=6/100 Zr), activity at constant metal to zirconium ratio (=4/100 Zr), and to examine the effect of varying dopant level (lithium and magnesium) on activity. A larger number of dopant atoms is required to attain the same level of oxygen vacancies as the valence of the dopant changes from +1 to +3.

Catalyst stability

The catalysts used for isobutylene synthesis showed no change in crystal structure under reaction conditions. Figures 3.20 through 3.23 show XRD patterns for catalysts after reaction. The maximum reaction temperature was always less than or equal to the calcination temperature. Therefore, changes in the phase before and after reaction were not expected.

Most catalyst samples were black when removed from the reactor. This color change occurred even for samples held at reaction conditions for the shortest time (~26 hours). When recalcined for one hour at 723 K (put in furnace hot) the catalysts returned to their original color. The black color was the result of both carbon and heavier hydrocarbon (coke) deposition. The carbon layer deposition will be discussed further in the *Catalyst Activity and Selectivity* section. The surface area is reduced by both coke deposition and thermal sintering. The relative importance of these two effects is indicated in Table 3.5. Comparison between the before reaction (B.R.), after reaction (A.R.), and recalcined (R.C.) columns of Table 3.5 shows that the precipitated catalysts experience a much larger decrease in surface area as a result of coke deposition.

As mentioned earlier, this loss of surface area was fairly consistent regardless of the time spent under reaction conditions. This indicates that a steady state is reached between coke deposition and coke reaction (cracking). The numbers in Table 3.8 are representative of nearly all catalysts (0.04-0.07 g_{coke}/g_{cat}). The second hydrothermal preparation had only ~0.009 g_{coke}/g_{cat}. This may have been the result of its reduced activity and shorter time on stream. This could also be the explanation for the lower value obtained with the calcination catalyst. Thermal sintering occurs at any temperature above absolute zero. The amount of sintering increases with both time and temperature. Platero and Mentruit (*48*) found that significant reduction in surface area of precipitated zirconia occurred at temperatures as low as 700 K. Since 700 K is only slightly above the reaction temperature used in the majority

of this study, some loss in surface area because of sintering is expected. The recalcined surface areas were generally 5-20% lower than the initial surface area (before reaction). The majority of surface area loss was caused by the coke deposition.

Surface areas of catalysts prepared by the hydrothermal and calcining methods were only slightly reduced after reaction. Recalcining these samples resulted in no change in the surface area. The difference in pore size between these catalysts and those prepared by the precipitated method may be the reason that coke deposition does not significantly affect surface area. Also, the reduced activity of these catalysts might contribute to surface area stability.

Catalyst Activity and Selectivity

The intralab reproducibility between the two fixed bed units was shown in the 1992 Contractors' Review Meeting Report. Because the two units yielded the same results for the same catalyst no reference is made in this report as to which unit was used to collect the data.

The experiments can be grouped into eight basic categories: (1) those that were performed to determine the optimal process conditions and catalyst, (2) those using modified sol gel catalysts with modified acid-base properties, (3) those involving hydrogen sulfide, (4) those using the oxygen vacancy theory catalysts, (5) the effect of gel *p*H, (6) the effect of temperature cycling, (7) those using the trickle bed reactor, and (8) those using the slurry reactor. Each of these groups will be discussed in a separate section. All hydrocarbon distributions in the following Tables are given in wt%. Appendix A gives the relationship between wt% and carbon conversion to each of the hydrocarbons. These numbers are essentially equivalent for the conversions achieved in this study.

Blank run

A blank run was conducted at 673 K, 50 atm, 1/1 CO/H_2 ratio, and a 90 second space time in a reactor packed with glass wool. The reactor was pretreated under flowing nitrogen for 18 hours. No reaction was detected under these conditions.

Experiments to determine optimum process conditions and catalyst preparation

Initial activity tests involved catalysts prepared by all methods. The results of initial activity tests for isobutylene synthesis over precipitated, hydrothermal, and calcination catalysts are shown in Figure 3.24. The manganese doped catalyst was almost completely inactive (cannot be shown on same scale with others). A report on the effect of manganese in reducing methane production in Fischer-Tropsch synthesis (*30*) motivated its investigation. Conversion was far below any of the other catalysts and the major product was methane. A possible explanation for the reduced activity and lack of typical isosynthesis product distribution may be that oxygen vacancy availability and mobility was reduced. Further discussion on this subject will be given in the section on oxygen vacancy catalysts.

Catalyst activity according to preparation method can be ranked as follows: (ppt.) > (CAL) > (HT). The catalysts prepared by the modified sol gel method were less active than the precipitated catalysts. However, increasing reaction temperature did not have an adverse effect on product distribution. The modified sol gel catalysts were run at a higher

temperature. A comparison between precipitated, commercial, and modified sol gel catalysts will be made at the end of this section. The results for isobutylene synthesis over the modified sol gel catalysts are given in the section on acid-base property modification. The 7% Ce-ZrO_2 was the most active and would be used in further activity/selectivity studies.

The effect of pressure on conversion at the same space time was minimal above 50 atm, but increasing pressure shifted the product distribution toward heavier hydrocarbons. These effects are illustrated in Figures 3.25 and 3.26. Pichler and Ziesecke (*7*) reported a similar trend with increasing pressure. They attributed the increase in conversion at higher pressures to the pressure itself, rather than the increased contact time associated with increasing pressure (same end gas flow rate).

In this work, the benefit of increased conversion at higher pressures was offset by the shift in hydrocarbon distribution toward the undesired C_5+ products. A pressure of 50 atm was chosen as the standard because the product distribution was favorable and space times as long as 150 seconds could be attained. As mentioned previously, Pichler and Ziesecke (*7*) obtained high CO conversions (50-90%), but their yield of isobutylene was low. The *iso*-C_4 fraction obtained by Pichler and Ziesecke was predominantly isobutane and a large percentage of the product was heavier hydrocarbons (46% at 723 K and 150 atm).

These two observations can be explained by the high pressure of the reaction. Higher pressure would favor production of alkanes and C_5+ products because the number of moles of reactant gases consumed per mole of product formed is greater than for alkenes and lighter hydrocarbons. Also Pichler and Ziesecke produced oxygenates (5%), even at 723 K. This can be attributed to thoria being a more basic oxide, since this study has found that the oxygenate to hydrocarbon ratio produced over acidified zirconia (*p*H of gel adjusted with HNO_3) is generally less than 0.05 (wt basis) at only 673 K. The most significant difference between this work and that of Pichler and Ziesecke is the decrease in undesired products (C_5+ hydrocarbons and oxygenates) while increasing isobutylene selectivity (up to 70% of C_4's) and maintaining a relatively high conversion.

Increasing temperature increased conversion, as expected, but also increased methane and isobutane formation. These effects are illustrated in Figures 3.27, 3.28, and 3.29. A CO conversion of 51% was achieved at 723 K, 50 atm, and 1/1 CO/H_2 over the cerium catalyst. The product, however, contained 60 wt% methane. The equilibrium constants for various reactions that can occur under isosynthesis conditions were given in Figure 1.1.

Methane is the thermodynamically favored product at all temperatures while saturated hydrocarbons are slightly favored over unsaturated hydrocarbons. Oxygenates are favored at lower temperatures as found by the methanol synthesis experiments. Thermodynamics can explain the increase in methane and isobutane formation with increasing temperature. The tradeoff between increased oxygenate production and increased methane production appeared to balance at 673 K. This temperature was chosen for most of the remaining activity/ selectivity studies over the precipitated catalysts. A temperature of 723 K was used in the majority of activity studies over the modified sol gel catalysts because of their reduced activity (discussed later). As mentioned earlier, the increase in temperature did not have a dramatic effect on methane production for modified sol gel catalysts.

Conversion was also found to be a function of CO/H_2 feed ratio with 1/3 > 1/1 > 2/1 (see Figure 3.30). In this work, interest was focused on hydrogen lean synthesis gas and 1/1 CO/H_2 was adopted as the standard.

Sodium, thorium, and cerium increased catalyst activity over undoped zirconia. It was reported (*10*) that cerium increased activity while retaining the selectivity of pure

zirconia and sodium decreased activity while increasing C_4 selectivity. Addition of thorium is expected to increase activity because pure thoria was found to be the most active isosynthesis catalyst (*7*). More discussion as to why these catalysts increased activity will be given in the section on oxygen vacancy catalyst results. The amount of titanium was decreased and thorium was added to the second hydrothermal preparation with the hope of increasing activity while retaining the same selectivity to *iso*-C_4 hydrocarbons.

Selectivity data for all fresh catalysts are shown in Table 3.9. These comparisons are made at almost equal conversions ($\sim$12%) to eliminate the effect of conversion on hydrocarbon distribution. Both pure zirconia and sodium doped zirconia produce mainly a C_5+ fraction. These two catalysts were not acidified in order to limit oxygenate production and the analysis did not account for oxygenates. Therefore, a significant portion of the C_5+ fraction could be dimethyl ether. Both dimethyl ether and methanol were injected independently and they both eluted in the column backflush (C_5+). In other cases dimethyl ether was the only oxygenate produced in detectable quantities and the dimethyl ether/hydrocarbon weight ratio was 0-4%.

Titanium was added to the precipitated zirconia with the hope of achieving the same *iso*-C_4 selectivity as in the hydrothermal case. However, the i-$C_4/\Sigma C_4$ ratio remained at about 70-75% for this catalyst. There was a shift in the hydrocarbon distribution for the two catalysts that were acidified. Both showed an increase in C_1-C_4 fraction and a decrease in C_5+ fraction. The i-$C_4/\Sigma C_4$ ratio for the 7% Ce-ZrO_2 was slightly lower because the higher activity of this catalyst resulted in production of more linear C_4's. In all cases greater than 90% of the i-C_4 fraction was isobutylene.

The catalyst prepared by the calcination method gave a hydrocarbon distribution similar to that of the precipitated catalysts that were acidified. The overall activity of this catalyst was about one-half (space time twice as long to get same conversion) that of the precipitated catalysts. The isobutylene fraction among i-C_4's was greater than 90% in this case also.

Both hydrothermally prepared catalysts gave $\sim$100% selectivity to the *iso*-C_4 compounds among C_4's produced (39% and 64% isobutylene respectively). The promotion of the *iso*-C_4 compounds over hydrothermally prepared catalysts could be related to the surface characteristics of the catalysts. Jackson and Ekerdt (*13*) suggested that branched C_4 hydrocarbons are formed by two independent paths. One involves condensation of a η^3-enolate (CH_3-$CH^{(-)}$-CH-O) with an adsorbed methoxide species and the other involves CO insertion in an η^3-enolate.

Though both routes lead to the formation of branched C_4's, different surface characteristics are required. The first is catalyzed by strong Lewis acid sites while the second is catalyzed by strong basic sites. The hydrothermal catalysts are more likely to have strong basic sites, since strong bases (sodium hydroxide and tetramethylammoniumhydroxide) were used in their preparation and they were not treated with acid. The hydrocarbon distribution was similar to that of precipitated catalysts. The C_5+ fraction increased when thorium was added in an attempt to increase activity. The overall activity of the hydrothermal catalysts was about one-third (space time three times as long to get same conversion) that of the precipitated catalysts. The unique selectivity to *iso*-C_4's may be a result of the larger pore size of the hydrothermal catalysts as compared with the precipitated catalysts.

Several characteristics were common to all catalysts. As space time increased the amount of methane increased and the ratio of isobutylene to isobutane decreased. The same

trends were noted as temperature increased. All of these observations can be explained in terms of thermodynamics. Catalysts showed a slight shift toward production of lighter hydrocarbons with time on stream although conversion remained constant. The modified sol gel catalysts showed the same trends with regard to pressure, temperature, and CO/H_2 ratio as described above.

A comparison of the precipitated zirconia with zirconia prepared by the modified sol gel (MSG) method and the commercial zirconia (H-0304) is shown in Table 3.10. The commercial and sol gel zirconias were evaluated at higher temperature and longer space times. The precipitated catalyst is much more active than either the commercial or modified sol gel catalysts (almost the same conversion at 50 K lower temperature and $\sim$½ the space time) and produces a larger C_4 fraction. The sol gel catalyst gave a higher selectivity to the *iso*-C_4 compounds.

Time on stream

The changes of catalyst performance with time on stream were studied over a thoria-zirconia catalyst. The catalyst was synthesized by a hydrothermal method. The procedure of experiments is shown in Figure 3.31. In the first 20 hours, the experiment condition was maintained at 723 K, 70 atm and 40 second space time, and two sets of data were taken at time on stream of 4 hours and 20 hours (*A* and *B* in Figure 3.31). Then a series of experiments were conducted at different space times, but still maintaining 723 K. At time on stream of 51 hours, the space time was again set to 40 seconds, and after 4 hours, a set of data was taken (*C* in Figure 3.31). Finally, after a series of experiments at different temperatures, reaction conditions were again set to 723 K, 70 atm and 40 s space time at 84 hours of time on stream, and after four hours, a set of data was taken (*D* in Figure 3.31).

Table 3.11 compares CO conversions and ratios of CH_4/iso-C_4's at different time on stream. Not much change in catalyst performance is observed for the first twenty hours when reaction condition was maintained constant (*A* to *B*). Even after fifty-five hours at the same temperature but different space times (*A* to *C*), the differences in CO conversion and weight ratio of CH_4 to iso-C_4's are within 10% of the first set of data. However, if temperatures were changed between the two set of experiments (*C* and *D*), the fraction of methane increased significantly. More discussion on the effects of temperature cycling on activity and selectivity will be presented later. However, our studies have shown that if a catalyst is held at the same reaction conditions the same level of activity and selectivity can be expected regardless of time on stream. Catalyst performance between catalyst batches synthesized in the same manner is also very reproducible.

Effect of CO cylinder

These experiments were performed in order to eliminate possible poisoning of the catalyst by iron carbonyls $\{Fe(CO)_5\}$ formed in the iron carbon monoxide cylinder. As described in the experimental section, the CO from the iron cylinder was passed though an activated charcoal bed and in some cases a commercial zirconia trap. However, use of the aluminum cylinder would eliminate the possibility of carbonyl formation in the cylinder. The tests were carried out over a fresh portion of the 7% cerium zirconia because it was the most active of the catalysts tested to that point. A comparison of results obtained using the iron and aluminum cylinders is shown in Table 3.12. Conversion is increased by about 10%

on a relative basis (i.e. 3 percentage points on an absolute basis) when using the aluminum cylinder.

This increase was realized in methane production with a corresponding decrease in C_4 production. The remainder of the hydrocarbon distribution (and C_4 distribution) was not significantly affected by using the aluminum CO cylinder. If the catalyst was being poisoned by iron carbonyls it was beneficial because the poison acted to reduce the amount of methane formed. However, qualitative analysis of several batches of catalyst for iron after reaction using the indicator thioglycolic acid showed no evidence that iron was being deposited on the catalyst.

Deposition of carbon layer on catalyst

Again, a 7% Ce-ZrO_2 was used (batch number 28) because it was the most active of the catalysts tested. This experiment was performed to quantify how much carbon was being laid down on the catalyst by the reaction $2CO \rightleftarrows C + CO_2$. This reaction is exothermic but is still highly favorable (K_{eq}=15700) at 673 K. The two observations that led to the question of whether this reaction was significant were (1) the black color of the catalyst after reaction and (2) during the first two hours after the reactor was brought on-line, the amount of CO_2 in the effluent could not be accounted for simply by the amount of hydrocarbons detected in the reactor effluent.

The catalyst was pretreated under flowing nitrogen (100 sccm) for 17 hours at 673 K and 35 atm. After pretreatment the reactor was bypassed and the carbon monoxide flow was started to flush the lines of nitrogen and obtain a flowrate and baseline area count for 100% CO from the GC. When these measurements were taken the reactor was brought back on-line. The experimental conditions were 673 K, 25 atm, and 90 second space time. A pressure of 25 atm was use to duplicate the partial pressure of CO under normal reaction ($CO + H_2$) conditions. Figure 3.32 shows the breakthrough curve for carbon monoxide. The sampling rate was one every 8 minutes.

The effluent was composed primarily of carbon monoxide and carbon dioxide; however, there were also traces of hydrocarbons present. Methane was present in decreasing amounts throughout the experiment (at most 0.005 mol%). The C_2 hydrocarbons were present through the first 4 hours and there were some C_3's present for about an hour. Hydroxyl groups on the catalyst might be the source of hydrogen for the hydrocarbons being produced. Carbon dioxide was still being produced after 12 hours but was less than 0.005 mole fraction. The majority of CO_2 was produced in the first 2 hours. When this catalyst was removed from the reactor it had turned dark brown, not completely black like catalysts subjected to $CO + H_2$ reactions.

The surface area after carbon deposition was 85 m^2/g (initially 88 m^2/g) which is much higher than that normally obtained for catalysts after reaction. When recalcined at 723 K for 1 hour some weight loss occurred and the catalyst returned to its original color. Approximately 0.0018 g_{carbon}/g_{cat} catalyst was lost. This is an order of magnitude less than that for catalysts where both CO and H_2 were fed (given earlier as between 0.04-0.07 g_{coke}/g_{cat}). The surface area after recalcining remained at 85 m^2/g, which showed that the surface area loss was the result of sintering and not carbon deposition. The volume of a monolayer of nitrogen as found by the BET method was 20.2281 cm^3/g for this catalyst. This corresponds to 5.44×10^{20} molecules of nitrogen per gram of catalyst.

The number of carbon atoms per gram of catalyst calculated from the weight of

carbon lost upon recalcination is 9.03×10^{19}. The van der Waals radius, defined as the closest approach between two atoms without forming a bond, for carbon is 1.85 Å (*43*). The area covered by one carbon atom (assuming spherical geometry) is 10.8 Å^2. The area of a nitrogen molecule assumed in the BET calculation is 16.2 Å^2. Thus, the number of carbon atoms deposited on the surface as determined from experiment is approximately 11% of that required to have monolayer coverage.

This experiment showed that carbon deposition occurred fairly quickly (~2 hours) and is not significant in reducing catalyst surface area compared with the accumulation of heavier hydrocarbons.

Modification of the acid-base properties

Method of preparation: The effect of method of preparation was examined by comparing zirconia prepared by the modified sol gel method to a commercial zirconia catalyst. ZrO_2 (MSG) is more active than ZrO_2 (H-0304), as shown in Figure 3.33. Since ZrO_2 (MSG) and ZrO_2 (H-0304) have about the same concentration of acidic sites on the surface, and differ only in the concentration of basic sites, the higher activity of ZrO_2 (MSG) is attributed to the increased amount of basic sites available for reaction. Figure 3.34 compares the CO reaction rates over the two catalysts. Each data point corresponds to a different space velocity. A linear regression gives a slope of 1.56. The concentration of basic sites are 0.00616 and 0.00333 mmoles per m^2 for ZrO_2 (MSG) and ZrO_2 (H-0304), respectively, and the ratio is 1.85, which is reasonably close to the slope of the line. The possible relation between the ratio of activities and the ratio of numbers of basic sites suggests that accessible basic sites are one of the requirements for an active isosynthesis catalyst.

The distribution of hydrocarbons is fairly close over ZrO_2 (MSG) and ZrO_2 (H-0304), except that the weight percent of heavy hydrocarbons is slightly higher over ZrO_2 (MSG) (Figure 3.35). The deviation from the Anderson-Schulz-Flory distribution for a standard polymerization reaction is apparent for isosynthesis when the distributions are plotted as Wt%/n *vs* n on a semi-log scale (Figure 3.36). For a standard polymerization reaction such as F-T synthesis, a straight line is obtained in the plot, whereas for isosynthesis, a discontinuity is observed at *n* of four. Another characteristic of isosynthesis is the large amount of branched products from the reaction (Figure 3.37). Both ZrO_2 (MSG) and ZrO_2 (H-0304) are selective for isobutene and isobutane, and iso-C_4 weight percent is slightly higher over ZrO_2 (MSG).

The comparison between ZrO_2 (MSG) and ZrO_2 (H-0304) indicates that the modified sol gel method can be used to synthesize zirconium oxide with a larger amount of basic sites on the surface, and consequently, higher isosynthesis activity. One of the keys in the modified sol gel preparation is the type of base used in making the soluble intermediate. Based on the experiments of this work, an organic base such as $(CH_3)_4NOH$ is preferred to an inorganic base such as NaOH to synthesize zirconia for isosynthesis.

Silica and Alumina: Figures 3.38 and 3.39 compare the isosynthesis activity of the three catalysts. Because of its lack of basic sites on the surface, SiO_2-ZrO_2 (MSG) is not active for isosynthesis. Previous work by Pichler and Ziesecke (*7*) also showed that silica is not an active isosynthesis catalyst. One might expect that Al_2O_3-ZrO_2 (MSG) is more active than ZrO_2 (MSG) because of the increased basicity, but in fact, the two catalysts have about the same activity. A possible explanation is the large concentration of aluminum on

the surface. Since Al_2O_3 itself is not active for isosynthesis (*4,7*), the increase of activity by enhanced basicity is probably offset by the decrease of surface zirconia available for reaction.

Pichler and Ziesecke (*7*) compared the isosynthesis activity of precipitated thoria and coprecipitated alumina-thoria, and concluded that the presence of alumina in the catalyst increased formation of methane and C_4 hydrocarbons and reduce formation of liquid hydrocarbons, but had no appreciable effect on carbon monoxide conversion. The same phenomena were observed in this work.

Alkali metals: The impact on methane and C_4 weight percent in hydrocarbons is not the same for all alkali metals (Figure 3.40): decreased methane production is observed over K-ZrO_2 (MSG), and increased C_4 production is observed for K-ZrO_2 (MSG) and Cs-ZrO_2 (MSG). In general, adding alkali metal promotes the production of heavy hydrocarbons ($C_{n>4}$), which is consistent with the observations in previous research (*4,7,15*). Except for Li-ZrO_2 (MSG) and Cs-ZrO_2 (MSG), alkali-promoted catalysts show higher selectivity to iso-C_4 hydrocarbons than for the unpromoted zirconia (Figure 3.41). The low activity of Na-ZrO_2 (MSG) is probably related to the high concentration of sodium on the surface.

Alkaline earth metals: The alkaline earth metals investigated improved the overall selectivity to iso-C_4 hydrocarbons (Figures 3.42 and 3.43). The distribution of C_4 hydrocarbons is not changed significantly (Figure 3.43), but C_4's consist of a larger portion of the total hydrocarbons than for the unpromoted zirconia (Figure 3.42). The majority of modified sol gel catalysts retained a significant level of activity after doping.

Level of dopant: The impact of promoter also depends on the level of loading. Figure 3.44 compares the hydrocarbon distributions for three catalysts with different calcium content. ZrO_2 (MSG) does not contain calcium, Ca-ZrO_2 (MSG), which has been discussed previously in this report, contains about 0.5 wt% calcium, and Ca(2%)-ZrO_2 (MSG) contains about 1.8 wt% calcium. Both Ca(2%)-ZrO_2 (MSG) and Ca-ZrO_2 (MSG) show improvement on hydrocarbon distribution (i.e, higher C_4 wt%) over ZrO_2 (MSG). Methane weight percent is the lowest for a high calcium loading (i.e., 2 wt%), and C_4 weight percent is the highest for a low calcium loading (i.e., 0.5 wt%). The distribution of C_4 hydrocarbons, however, remains fairly constant regardless of the calcium loading, as shown in Figure 3.45. More discussion on doping with lower valence cations and level of doping is given in the section on oxygen vacancy catalysts.

Effect of co-feeding hydrogen sulfide and presulfiding

The motivation for using hydrogen sulfide was the possible reduction in methane formation that might occur because of selective poisoning by sulfur. The 7% cerium zirconia was utilized for these experiments as well. Batch number 6 was used in the non hydrogen sulfide cases while batch number 8 was used when hydrogen sulfide was co-fed. Additionally, a hydrogen sulfide free run was performed over batch 8 as an activity check. Batch number 28 was used for the presulfiding experiment.

The effect of hydrogen sulfide on methane, total C_4, and C_5+ production rates are shown in Figure 3.46. The decrease in methane production rate is a result of an increase in C_5+ production rate, while total C_4 production is slightly increased. The CO conversions at 60 second space time are statistically the same (first two columns under 'without H_2S' heading, Table 3.13) between the two batches.

The product distribution is shifted slightly toward methane and C_5+ with C_4's

reduced for the first batch (second column). Possible explanations for the difference in product distribution (more methane and less oxygenates) could be that batch 6 experienced a slightly lower *p*H or slightly higher calcination or reaction temperature. However, the performance for hydrogen sulfide free runs between batches is similar enough to allow meaningful comparison between hydrogen sulfide free and hydrogen sulfide runs ignoring the slight difference in selectivity between catalyst batches. ZrO_2 is apparently unaffected by hydrogen sulfide as found for ThO_2 by Pichler and Ziesecke (*7*).

The most striking effect of co-feeding hydrogen sulfide is the drastic increase in C_5 production, particularly 3-methyl-1-butene (Tables 3.13 and 3.14). In Table 3.14, the C_5 hydrocarbons are divided into three groups: (1) 3-methyl-1-butene, (2) 2-methyl butane, 1-pentene, 2-methyl-1-butene, and (3) *n*-pentane, *trans*-2-pentene, *cis*-2-pentene, 2-methyl-2-butene. This grouping is based on boiling points and the separation capability of the Porapak Q column in the on-line SRI GC. These groupings are consistent with GC results for injection of standards. Analysis of the C_5 fraction is not possible on the other two gas chromatographs. Thermodynamics show that 3-methyl-1-butene is the least favorable of the branched C_5 alkenes (*24*). Table 3.15 gives the Gibbs free energy of formation for the C_5 alkanes and alkenes.

Overall, 1-pentene is the least favorable C_5 compound but has a very similar ΔG_f° to 3-methyl-1-butene. The 2-methyl alkenes and *cis*- and *trans*-2-pentenes are the major C_5 products for isosynthesis over zirconia just as isobutylene and *cis*- and *trans*-2-butene are the major C_4 products (see Table 3.13). Thus, the second and third groups dominate the C_5 distribution and only a slight amount of the thermodynamically unfavorable 3-methyl-1-butene is formed. When hydrogen sulfide is included, 3-methyl-1-butene composes almost 75% of the C_5 product (Table 3.14). The other two C_5 groups are formed in the same ratio as for the hydrogen sulfide free case. The dramatic increase in C_5 production with hydrogen sulfide could be a result of suppression of chain growth to heavier (C_{10}+) hydrocarbons as was speculated by Nakajo *et al.* (*49*) for acetic acid selectivity, a suppression of C_5 cracking to C_2's and C_3's since a noticeable drop in C_2 and C_3 production occurred, or a decrease in adsorption strength between the catalyst and 3-methyl-1-butene (possibly initial product) that allows it to desorb from the surface before it can react further to the more thermodynamically favored 2-methyl butenes. In this case suppression of chain growth does not mean that the C_6+ fraction cannot increase (as shown in Table 3.13). It is suggested that more of the C_5-C_9 hydrocarbons were formed at the expense of C_{10}+'s when hydrogen sulfide was co-fed.

The effect of increasing space time at constant temperature and pressure under hydrogen sulfide is shown in Table 3.13. The selectivity change is the same as that for the hydrogen sulfide free case. Methane increases (as dictated by thermodynamics) and C_5+ decreases. The C_4's also show a slight increase, but this is because more isobutane is being produced (also expected from thermodynamics). The only oxygenates produced were dimethyl ether and methanol and their production was fairly constant with increasing space time.

Table 3.16 shows the activity and selectivity changes that occur with hydrogen sulfide with changing temperature. It should be noted that the order these experiments were performed is not that of increasing temperature. The base case at 673 K was run first, followed by runs at 698 K, 723 K, and finally 648 K. This is the reason the conversion is lower and more methane and isobutane were produced at 648 K than would be expected from examining data at 673 K, 698 K, and 723 K. It is also the reason the base temperature was

not revisited after each excursion. An experiment at the base temperature was performed after those at 698 K, 723 K, and 648 K. The carbon monoxide conversion, methane wt%, and isobutane wt% among C_4's were 18.33, 38.03, and 30.77, respectively. These numbers can be compared to those in the first column of Table 3.13 to support the previous observation.

As temperature is increased, methane and C_4 alkane selectivity increase, as expected from thermodynamics. Throughout these experiments the mass balance on sulfur (as hydrogen sulfide) was always much less than 100%. The sulfur balance (mass sulfur out/mass sulfur in) was 0.015 (~98.5% of sulfur fed was not seen as hydrogen sulfide in the product stream), 0.032, 0.158, and 0.468 for 648 K, 673 K, 698 K, and 723 K respectively. As detailed in the experimental section, the feed composition is checked before each experiment by bypassing the reactor.

The area count for hydrogen sulfide on the GC was comparable to that obtained by injecting the mixture directly into the GC with a syringe. Sufficient time was allowed for the area count to reach a steady value indicating that the system has been conditioned to hydrogen sulfide. Therefore, the poor closure on sulfur was the result of reactions with the catalyst and not with the system components (i.e. tubing and fittings). The amount of hydrogen sulfide (and other products) in the effluent was steady over the course of the experiment.

One possibility for this lack of closure is the formation of liquid compounds containing sulfur. Even though no new peaks were observed on the SRI GC, which is before the liquid trap, the sulfur containing compound would be present in such a small quantity (mass of sulfur fed <1.5% of total mass fed) that it would be undetectable or masked by another product peak.

The fact that the sulfur balance improves with increasing temperature shows that less hydrogen sulfide is being adsorbed at higher temperatures (as expected). This is also reflected in the decrease in C_5+ fraction with increasing temperature and the decrease in 3-methyl-1-butene selectivity. At 648 K, 3-methyl-1-butene composes over 94% of the C_5 product. As temperature increases, thermodynamics and the reduced amount of sulfur adsorbed combine to shift the C_5 product distribution to 2-methyl butane (lowest ΔG_f°). Still, even at 723 K, 3-methyl-1-butene production is much higher than the hydrogen sulfide free case at 673 K which shows that adsorbed sulfur is continuing to affect the selectivity. This is also evident in the relative amounts of C_2+C_3 and C_5+ produced. In a hydrogen sulfide free case the wt% among hydrocarbons for these two fractions was 14.7 and 10.3, while with hydrogen sulfide they are 9.0 and 14.6 respectively at 723 K.

For the presulfiding experiment the catalyst was pretreated in the usual way. The presulfiding procedure was similar to that for the carbon deposition experiment (673 K, 25 atm, 90 second space time) except that the 1.06% H_2S in H_2 mixture was used. The breakthrough curve for H_2S is shown in Figure 3.47. Hydrogen sulfide was adsorbed for about 21 hours. Extrapolating this curve to $C/C_o=1.0$ would give ~48 hours for saturation. The flow rate of H_2S during presulfiding was 9.766×10^{-4} mol/hr and the area above the breakthrough curve is 339.33 minutes. This gives the total moles of H_2S adsorbed as 5.523×10^{-3}, or 3.326×10^{21} molecules. The total weight of catalyst was 11.0892 grams. Thus, there was 3.00×10^{20} molecules of H_2S per gram of catalyst. This corresponds to ~55% of monolayer coverage if the area covered by an H_2S molecule is assumed to be the same as that covered by a nitrogen molecule.

After 21 hours of presulfiding the reactor was brought off-line and the carbon

monoxide flow was started. The feed flow rate and composition [CO and (H_2+H_2S)] were checked and then the reactor was brought back on-line. Analysis began 22 hours later. The results are shown in Table 3.17. It should be noted that the runs without presulfiding were done using the aluminum CO cylinder while the run with presulfiding was not. This would cause the conversion difference between the two runs to decrease by ~3 percentage points. Even with this correction the conversion with presulfiding is lower at equal (90 second) space times. The 60 second space time run without presulfiding is included to allow comparison at equal conversions. The C_5, isobutylene, and 3-methyl-1-butene fractions are higher for the presulfided catalyst.

This catalyst was black after reaction as well. When recalcined at 723 K for one hour a weight loss of 0.0147 g_{coke}/g_{cat} occurred. This is 3-5 times less than the weight loss normally experienced by other catalysts. Batch number 8 in Table 3.8 was the catalyst used in non presulfiding experiments. It appears that presulfiding reduces the amount of coke deposition on the catalyst possibly by reducing adsorption strength between the catalyst and products. The increase in isobutylene and 3-methyl-1-butene could also be explained by reduced interactions between the catalyst less favorable alkene products.

An injection 1 hour after bringing the reactor on-line showed that more H_2S was in the effluent than was being fed. This indicated that some of the previously adsorbed H_2S was being desorbed by CO (and H_2). After the reaction had reached steady state the amount of sulfur in the effluent (as H_2S) was ~5% of that being fed. This is similar to the non presulfiding run in which this number was ~3%. Again, it is most likely that the sulfur is being incorporated into a liquid compound or that the compound is present in very small amounts.

Sulfur analysis of batch number 8 (co-feeding H_2S) after reaction and after recalcination indicated ~0.9 mg sulfur per gram of catalyst. This equates to 1.69×10^{19} molecules of sulfur per gram of catalyst. Based on equal area covered as compared with nitrogen this represents ~3% of monolayer coverage. This shows that a majority of sulfur adsorbed during presulfiding is desorbed under reaction conditions, but this small amount of sulfur still has a significant effect on the product distribution.

Effect of oxygen vacancies

The results of all activity tests are shown in Table 3.18. The description for each run indicates the dopant and amount of dopant used (e.g. LiZ04 refers to catalyst with Li/Zr ratio of 0.04). The catalysts used (batch numbers 9-22, and 24) in the vacancy study can be divided into three groups: (1) single dopant - zirconium vacancies, (2) single dopant - oxygen vacancies, and (3) multiple dopants - oxygen vacancies. The tantalum doped zirconias belong to the first group. As seen in Table 3.18, the two tantalum doped catalysts are relatively inactive compared to the others. The more heavily doped sample is almost completely inactive. A much lower ionic conductivity was noted for zirconia doped with Ta_2O_5 (*50*) and was attributed to the Ta^{+5} cations acting as vacancy suppressors.

What this really means is that the tantalum doped zirconias contain zirconium vacancies instead of oxygen vacancies. Since conduction occurs by vacancy migration, both the availability and mobility of the vacancies influence the ionic conductivity. Geometric considerations may explain the decrease in conductivity for zirconias doped with higher valence cations. For anion migration the gaps between the cations are 90% as large as the anions themselves while for cation migration the gaps are only 56% of the cation size (*50*).

The ease of anion mobility compared with cation mobility is also evident in calculations performed by Mackrodt and Woodrow (*44*) in which the activation energy for a free anion vacancy jump was found to be ~63 kJ/mol while that for a free cation vacancy jump was ~826 kJ/mol. The fact that the activity decreased significantly as oxygen vacancies disappeared supports the theory that oxygen vacancies are the active catalytic sites (*13,47,51*). Also, the decreased selectivity to C_4's suggests that oxygen vacancies play a vital role in the selectivity of the isosynthesis reaction. The reduced selectivity to C_4's is not a conversion effect.

All of the single component doped catalysts (that created oxygen vacancies) were active toward isosynthesis. Figure 3.48 shows the comparison between undoped zirconia and those doped with lithium, magnesium, aluminum, and dysprosium. Some of the catalysts are more active than the pure zirconia while some of them are less active as found by Jackson and Ekerdt (*13*). The lithium doped catalyst shows higher activity at lower dopant concentration and levels off at higher dopant concentrations. Since lithium introduces the highest number of oxygen vacancies per lithium atom incorporated into the lattice and has the highest negative charge (-3) of any of the lower valence ions there is increased interaction between the oxygen vacancy and the lithium cation as lithium concentration increases. This could lead to a decrease in the overall vacancy mobility and thus to a decrease in activity. Activity reaches a steady value because the benefit of increased numbers of oxygen vacancies at higher dopant levels is counteracted by increased binding of the vacancies to the dopant cations. The largest activity for lithium doped catalysts may lie in the 0 to 4 Li/100 Zr dopant range.

The magnesium doped catalysts show a maximum in activity around 9 to 10 Mg/100 Zr (≈9 mol% MgO). A maximum in isosynthesis profile also occurs in this same concentration range. This is consistent with results of Jackson and Ekerdt (*13*) for isosynthesis and Etsell and Flengas (*50*) for ionic conductivity. The maximum in C_4's which also occurs at this dopant level lend support to the conclusion that the selectivity of the isosynthesis catalysts are directly related to the oxygen vacancy availability and mobility as well. A maximum occurs because of the tradeoff between the increasing number of oxygen vacancies present and increasing hindrance of vacancy mobility.

The samples doped with +3 cations show somewhat lower activity than the lithium- and magnesium-doped catalysts. Since only two batches of aluminum and dysprosium doped catalysts were tested it is not clear where the maximum in activity occurs, but it appears to lie in the 6 to 10 M/100 Zr range for both dopants. The lower activity of the aluminum doped zirconia might be attributed to all of the alumina not dissolving in the zirconia phase. However, since the XRD patterns did not indicate a second phase and the alumina mole percent was relatively low (2-6%), the reduced activity was more likely the result of stronger interactions between the oxygen vacancies and the small aluminum cation. The reduction of activity in the dysprosium samples may be attributed to a steric blocking effect of vacancy migration by the larger dysprosium cation.

Figure 3.49 shows the effect of dopant ionic radius on activity at a constant level of oxygen vacancies. An apparent maximum near the radius of zirconium (0.814 Å) lends support to findings that the highest ionic conduction would be obtained with dopant similar in size to zirconium (*52-57*). Figures 3.50 and 3.51 show the relationship between activity and the dopant charge to ionic radius ratio at constant oxygen vacancies and constant dopant to zirconium ratio respectively. Both of these show activity to increase with decreasing charge to radius ratio. One might expect a +1 dopant to be less active because of the

increased attraction between an oxygen vacancy (+2) and the -3 charge of the dopant in the zirconium lattice site. However, recall that the +1 dopant introduces the most oxygen vacancies per dopant atom (Table 3.7) so a lower concentration of dopant is required for the same level of oxygen vacancies as +2 and +3 dopants. The lower concentration would actually reduce the amount of interaction between oxygen vacancies and dopant cations leading to an increase in activity (conductivity). Low concentrations of a lower valence cation with radius similar to that of zirconium may be the optimum design for single component doped zirconia catalysts.

The product distribution was not significantly affected by any of the lower valence dopants (see Table 3.18). This is particularly interesting in that for most reactions the properties of the additives usually have a noticeable effect on product distributions. In the case of isosynthesis it seems that the vacancies are more important than the dopant. Slightly more methane and less C_5+ was produced over the doped zirconias as compared to the pure zirconia. This may be attributed to an increase in catalyst acidity because of the introduction of electron accepting oxygen vacancies. Also, the +3 dopants produced more oxygenates (methanol and dimethyl ether) than the +1 or +2 dopants. For dysprosium, the explanation may be that Dy_2O_3 is a more basic oxide than ZrO_2. However, since alumina is more acidic the reason for increased oxygenate production over aluminum doped catalysts is unclear.

The final group consists of the yttrium, barium, copper '123' doped zirconia. As mentioned, the motivation for studying this catalyst was the possibility of increasing activity because of increased oxygen vacancy mobility. Table 3.18 gives the results for the two runs performed over this catalyst. Run YBCZ was done with the standard CO/H_2 feed while run YBCZS was performed using a feed of CO and the 1.06% H_2S in H_2 mixture.

A 43% increase in CO conversion over that obtained with the pure zirconia catalyst was achieved for run YBCZ. This increase in conversion was realized as an increase in methane production. Also, the *iso*-C_4 distribution favored isobutane over isobutylene. The increase in methane production could be attributed to the copper which is a component of low temperature methanol synthesis catalysts. The formation of isobutane instead of isobutylene is the result of a more acidic catalyst caused by the increase in oxygen vacancy availability and mobility. The large increase in conversion strengthens the theory that active catalysts have a high degree of oxygen vacancy availability and mobility.

Hydrogen sulfide was added to the feed because of its previously found effect on product distribution. A 33% increase in CO conversion over the non-H_2S case (90% increase over the pure zirconia catalyst) was achieved while co-feeding H_2S. This increase in conversion was not expected since the previous studies had shown that H_2S did not affect activity. Hydrogen sulfide may have caused an increase in oxygen vacancy mobility possibly by incorporation of S^{-2} into the zirconia lattice. No change in the XRD pattern was observed that might indicate the formation of another phase. Again, this increase was realized in methane production ($\sim$74 wt% of hydrocarbon product). The fraction of isobutane in the C_4's was even larger than for the non-H_2S case. This implies that the acidity of the catalyst was enhanced by the addition of H_2S. The C_5 fraction did increase with the addition of H_2S and 3-methyl-1-butene selectivity went from $\sim$0 to 50 wt% (among C_5's). However, this slight increase in C_5 fraction was dwarfed by the huge increase in methane. The small amount of oxygenates produced when pure hydrogen was used and complete disappearance with hydrogen sulfide supports the conclusion that the '123' zirconia was more acidic than pure zirconia and that this acidity was enhanced by the addition of H_2S.

Effect of gel pH

These experiments used batches 9 and 25-27 (see Table 3.5). These gels were adjusted to *p*Hs of 7.0, 10.0, 8.5, and 5.5 respectively. Catalytic activity was slightly affected by *p*H. The conversion over zirconia at *p*H 5.5 and 10.0 was statistically the same. The conversion over zirconia at *p*H 7.0 was slightly lower, while that at *p*H 8.5 was ~15% higher. The amount of oxygenates produced was expected to increase with increasing *p*H. The largest amount of oxygenates were produced over the zirconia adjusted to *p*H 10.0, but no clear trend in oxygenate production with *p*H was evident. Figures 3.52 and 3.53 show that the isobutylene to isobutane ratio, isosynthesis profile [$C_4/(C_2+C_3)$], isobutylene fraction among C_4's, and isobutylene to methane ratio increased with increasing *p*H (basicity).

Jackson and Ekerdt (*13*) found that high isosynthesis profiles were associated with more acidic catalysts. One possible explanation for the conflict is that Jackson and Ekerdt's data are at very low conversions (<2%). It is well known that conversion can have a significant effect on product distribution. Jackson and Ekerdt also found that the amount of C_1 produced was larger for catalysts with lower isosynthesis profiles. The same trend is observed here, the wt% of methane decreases with increasing isosynthesis profile (basicity). The isobutylene to methane ratio increased with *p*H because the isobutylene fraction increased and methane decreased. The isobutylene to isobutane ratio increased with increasing *p*H possibly because hydrogenation was reduced with decreasing acidity. Isobutylene and isobutane were the only C_4 components to show a significant change in amount produced with *p*H.

Effect of temperature cycling

As mentioned earlier, the catalytic activity decreased and the hydrocarbon distribution shifted toward the more thermodynamically stable products with any temperature cycling. These effects for the 7% Ce-ZrO_2 catalyst are shown in Table 3.19. The first column (Fresh) in Table 3.19 is for a batch of catalyst loaded into the reactor and subjected to normal pretreatment procedures. Both 60 and 90 second space times are shown for the fresh catalyst for comparison with the cycled and reheated catalyst. The second column is the result for the same catalyst after the temperature cycle 673 K → 698 K → 723 K → 673 K. These experiments (Fresh and Cycled) were performed using the iron CO cylinder while the other two were performed using the aluminum CO cylinder.

The important point is how the conversion and product distribution change with temperature cycling. After the temperature cycle the catalyst is slightly less active (~7%) and the product distribution has shifted to producing a majority of methane. Also the distribution among the C_4 has shifted to the alkanes with isobutane showing about a 50% increase. The third column (Reheat) gives the result for a fresh catalyst subjected to a more extreme temperature cycle (300 K → 673 K → 300 K → 673 K → 300 K → 673 K).

Throughout this cycle nitrogen was passed over the catalyst at pretreatment conditions. Again, there was catalyst deactivation (more severe in this case) and a dramatic shift toward methane. The final column (Reheat w/H_2S) is the result for the same catalyst while co-feeding hydrogen sulfide. The conversion is only slightly affected by adding hydrogen sulfide, but the product distribution is significantly changed. Methane and C_2+C_3 are reduced by almost half while C_5+ shows a threefold increase. As found before, this increase is the result of an huge increase in 3-methyl-1-butene production.

The product distribution is extremely sensitive to the temperature to which the catalyst has been subjected. With increasing temperature, the thermodynamically favored products increase regardless of the temperature at which the experiment is performed. In other words, once the catalyst is subjected to a certain (higher) temperature the product distribution achieved at that temperature persists even at lower temperatures. Evidence of this is seen in Table 3.19. Even though the 'reheated' catalyst underwent a more severe temperature cycle it produced less methane than the catalyst that was cycled to 723 K because the highest temperature it was subjected to was only 673 K. Possibly the catalyst active sites are altered with temperature cycling and change more significantly as the temperature is increased. Hydrogen sulfide somehow overrides the temperature effect on product distribution and the catalyst behaves as if no temperature cycling occurred, except for the loss in activity.

Trickle bed reactor

The commercial zirconia was evaluated in the reactor system, which can be operated as a fixed bed gas phase or as a trickle be reactor. Decalin was determined to be the best oil to use for the trickle bed experiments. Linear hydrocarbons hydrocracked over the zirconia at the temperature of the isosynthesis.

A comparison of the performance of the catalyst when operating the reactor in the fixed and trickle bed modes at 669 K and 51 atm is shown in Figures 3.54 and 3.55. The selectivity for isobutylene and the C_4 components was higher when operating the reactor as a conventional gas phase fixed bed reactor than when operating the reactor as a trickle bed. The CO conversion was approximately the same for both modes of operation. The product distribution obtained with the trickle bed contains more C_3's, less methane, less C_4's, and less C_5+ than the product distribution obtained when operating in the gas phase fixed bed reactor mode.

These experiments indicated that mass transfer resistances were occurring in regard to the propagation of the hydrocarbon chain. A greater amount of propylene is produced in the trickle bed than with the fixed bed gas phase reactor. The separator temperatures and oil flow rates were shown to have minor effects on the product distribution. Figures 3.56 through 3.59 illustrate the effects of the oil flow rate and separator temperature on the product distribution. Figure 3.59 shows that as oil flow rate increases propylene decreases and C_4 and C_5 production increases.

Slurry reactor

All of the previous studies on isosynthesis have been conducted in gas-solid fixed bed reactors. Using a three phase gas-oil-catalyst slurry reactor for isosynthesis can have certain advantages. Primarily, the reaction can be run in the absence of mass transfer limitations. There is evidence in the literature (*12*) that the isosynthesis reaction becomes controlled by external mass transfer at temperatures above 723 K. Continuous circulation of the oil phase may enable separation of light components from the heavy components (C_5+ which are produced by the reaction) at the gas oil separator. The heavy components can be circulated back to the reactor dissolved in the oil and be further converted into light hydrocarbons. In addition, selectivities for the desired products can be increased because of the effect of perfect mixing compared to plug flow. The CO/H_2 ratio in the oil phase may also be quite different than the CO/H_2 ratio in the feed gas because of the differences in Henry's law

constants for hydrogen and carbon monoxide which may affect the product distribution.

Both the commercial zirconia and a precipitated zirconia were used in the slurry reactor studies. The commercial and precipitated catalysts had surface areas of 50 and 92 m^2/g, respectively. Experiments with the commercial zirconia used an oil flow rate of 0.04 g/sec while those with the precipitated zirconia used and oil flow rate of 0.08 g/sec. In both cases 10 cm^3 of catalyst and 60 cm^3 of oil were used.

A time on stream study was conducted to determine if there was any catalyst deactivation. Deactivation was not expected because of the stability of the zirconia as found in the fixed bed experiments. As seen in Figure 3.60, a slight increase in conversion was observed over a period of 17 hours. Figures 3.61 and 3.62 show the comparison of the hydrocarbon and C_4 distributions for the slurry and fixed bed reactor configurations over ZrO_2 (ppt.). Although the CO conversion, at equal inlet flowrates, is lower for the slurry reactor case, the selectivities to C_4 products are higher. Figures 3.63 and 3.64 show the comparison of the hydrocarbon and C_4 distributions for different CO/H_2 ratios over the commercial zirconia. Figure 3.65 shows the change in hydrocarbon distribution with CO/H_2 ratio over ZrO_2 (ppt.).

The mass transfer resistances were calculated based on the data using the procedure outlined by Smith (*58*). Gas bubble to liquid mass transfer coefficients were calculated using the Calderbank and Moo-Young correlation (*59*) and liquid to particle mass transfer coefficients were calculated using the correlation given by Brian *et al.* (*60*). The effectiveness factors were found to be very close to unity. Therefore, it is believed that the reactions were run in the kinetically controlled regime in the absence of any mass transfer limitations.

The experiments with the commercial zirconia were conducted at a slightly higher temperature (679 K instead of 673 K) and lower space velocities (400 hr^{-1} instead of 1050 hr^{-1}) because of the considerably lower activity of this catalyst compared to the zirconia prepared in our laboratory by precipitation. Tables 3.20 through 3.25 give the experimental conditions for run results presented in Figures 3.60 through 3.65.

Equation Development for the Modeling of Carbon Monoxide Conversion (Fixed Bed)

The following equation development is done strictly on an empirical basis. The physical meaning of the parameters obtained from the fit of the data and possible simplified mechanisms that give the final form of the rate equation are discussed in Appendix B.

Alkenes as predominant products with CO_2 inhibition

The reaction to form alkenes may be written as

$$\underset{(A)}{2nCO} + \underset{(B)}{nH_2} \rightleftarrows \underset{(C)}{C_nH_{2n}} + \underset{(D)}{nCO_2}$$

The design equation for a plug flow reactor is

$$-\frac{dn_A}{dW} = r_A = \frac{k_p p_A^a p_B^b}{\left(1 + K_{CO_2} p_D\right)^c} \tag{3.1}$$

The mole balances for the given reaction are written in terms of conversion of carbon monoxide.

$$\begin{aligned} n_A &= n_A^o - n_A^o x \\ n_B &= n_B^o - \frac{1}{2} n_A^o x \\ n_C &= n_C^o + \frac{1}{2n} n_A^o x \\ n_D &= n_D^o + \frac{1}{2} n_A^o x \\ \hline n_T &= n_T^o + n_A^o x\left(\frac{1}{2n} - 1\right) \end{aligned} \tag{3.2}$$

If k_p is divided out of the design equation then

$$-\frac{dn_A}{dW} = \frac{p_A^a p_B^b}{\left(q + s p_D\right)^c} \tag{3.3}$$

where

$$q = \frac{1}{k_p^{1/c}} \qquad s = \frac{K_{CO_2}}{k_p^{1/c}} \tag{3.4}$$

Partial pressures may be written in terms of moles and total pressure as follows

$$p_i = \frac{n_i}{n_T} P \tag{3.5}$$

The partial pressures can be written in terms of conversion by substituting the mole balances (3.2) into the above expression and defining β as the feed ratio of hydrogen to carbon monoxide.

$$p_A = \frac{(1-x)}{\left[1+\beta+x\left(\frac{1}{2n}-1\right)\right]}P$$

$$p_B = \frac{\left(\beta-\frac{1}{2}x\right)}{\left[1+\beta+x\left(\frac{1}{2n}-1\right)\right]}P \qquad (3.6)$$

$$p_D = \frac{\frac{1}{2}x}{\left[1+\beta+x\left(\frac{1}{2n}-1\right)\right]}P$$

The left hand side of the design equation (3.3) is written in terms of conversion and space time (τ) according to the following (where ρ_b is bulk density).

$$dn_A = -n_A^o dx \qquad (3.7)$$

$$n_A^o = \frac{p_A^o v_o}{RT_o} \qquad (3.8)$$

$$W = \rho_b V \qquad dW = \rho_b dV \qquad (3.9)$$

$$\tau = \frac{V}{v_o} \qquad (3.10)$$

The left hand side of the design equation can now be expressed as

$$-\frac{dn_A}{dW} = \left[\frac{P}{(1+\beta)\rho_b RT_o}\right]\frac{dx}{d\tau} \qquad (3.11)$$

The complete differential equation describing how conversion changes with space time is written by combining Equations (3.3), (3.6), and (3.11) and is given by

$$\frac{dx}{d\tau} = \frac{\rho_b RT_o P^{a+b-1}(1+\beta)(1-x)^a(\beta-\frac{1}{2}x)^b}{M^{a+b-c}N^c} \qquad (3.12)$$

where

$$M = \left[1 + \beta + x\left(\frac{1}{2n} - 1\right)\right] \tag{3.13}$$

$$N = \left[q\left(1 + \beta + x\left(\frac{1}{2n} - 1\right)\right) + s\frac{xP}{2}\right] \tag{3.14}$$

Alkenes as predominant products with CO inhibition

The design equation for this case is

$$-\frac{dn_A}{dW} = \frac{p_A^a p_B^b}{(q + s p_A)^c} \tag{3.15}$$

The development of equations for mole balances, partial pressures, and the left side of the design equation is the same as for the case with CO_2 inhibition. Substitution of these equations into the design equation gives

$$\frac{dx}{d\tau} = \frac{\rho_b R T_o P^{a+b-1}(1+\beta)(1-x)^a(\beta - \frac{1}{2}x)^b}{M^{a+b-c} N^c} \tag{3.16}$$

where

$$M = \left[1 + \beta + x\left(\frac{1}{2n} - 1\right)\right] \tag{3.17}$$

$$N = \left[q\left(1 + \beta + x\left(\frac{1}{2n} - 1\right)\right) + s(1-x)P\right] \tag{3.18}$$

Alkanes as predominant products with CO_2 inhibition

The reaction to form alkanes may be written as

$$\underset{(A)}{2nCO} + \underset{(B)}{(n+1)H_2} \rightleftarrows \underset{(C)}{C_nH_{2n+2}} + \underset{(D)}{nCO_2}$$

The design equation (3.3) is used with the following mole balances

$$
\begin{aligned}
n_A &= n_A^o - n_A^o x \\
n_B &= n_B^o - \left(\frac{n+1}{2n}\right) n_A^o x \\
n_C &= n_C^o + \frac{1}{2n} n_A^o x \\
n_D &= n_D^o + \frac{1}{2} n_A^o x \\
\hline
n_T &= n_T^o - n_A^o x
\end{aligned}
\tag{3.19}
$$

The partial pressures become

$$
\begin{aligned}
p_A &= \frac{(1-x)}{[1+\beta-x]} P \\
p_B &= \frac{\left(\beta - \frac{n+1}{2n} x\right)}{[1+\beta-x]} P \\
p_D &= \frac{\frac{1}{2} x}{[1+\beta-x]} P
\end{aligned}
\tag{3.20}
$$

The complete differential equation describing how conversion changes with space time is written by combining Equations (3.3), (3.11), and (3.20) and is given by

$$
\frac{dx}{d\tau} = \frac{\rho_b R T_o P^{a+b-1} (1+\beta)(1-x)^a (\beta - \frac{n+1}{2n} x)^b}{M^{a+b-c} N^c} \tag{3.21}
$$

where

$$
M = [1 + \beta - x] \tag{3.22}
$$

$$
N = \left[q(1 + \beta + x) + s \frac{xP}{2} \right] \tag{3.23}
$$

Alkanes as primary products with CO inhibition

The design equation (3.15) is used with mole balances (3.19) and partial pressures (3.20) as derived above. The final differential equation for describing how conversion changes with space time is

$$\frac{dx}{d\tau} = \frac{\rho_b R T_o P^{a+b-1}(1+\beta)(1-x)^a(\beta - \frac{n+1}{2n}x)^b}{M^{a+b-c}N^c} \qquad (3.24)$$

where

$$M = [1 + \beta - x] \qquad (3.25)$$

$$N = [q(1 + \beta + x) + s(1-x)P] \qquad (3.26)$$

Results of Modeling of Carbon Monoxide Conversion (Fixed Bed)

The parameters q and s (and thus k_p and K_{CO_2}) were found using the SimuSolv® Modeling and Simulation Software developed by Dow Chemical Company. The routine uses numerical integration to solve the ordinary differential equation and maximizes a log-likelihood function to find the best fit between experimental and predicted data. More details can be found in the *SimuSolv® Reference Guide*.

Model discrimination

Initially, an attempt was made to fit the data using the design equation incorporating olefin formation and CO_2 inhibition (equation 3.1) but with c=0 (no CO_2 inhibition). Figure 3.66 illustrates the poor prediction that is achieved when CO_2 inhibition is not included. Also shown in this figure is the CO_2 inhibited fit. In this case an excellent fit of the data is obtained with a=1, b=0.5, c=1, and n=4. An equivalent fit of the data was obtained for a=1, b=0.5, c=2, and n=4. As mentioned previously, discussion of the parameters is given in Appendix B. The simpler equation (a=1, b=0.5, c=1) was utilized in the remainder of the modeling work.

The effect of n on the fit is shown in Figure 3.67. The difference in fit between n=4 and n=1 is not significant. Thus, a value of n=4 (C_4 products predominant) was adopted as the standard. The design equation in which alkanes are the primary products (Equation 3.21) was used in preparing Figure 3.67 while that in which alkenes are the primary products (Equation 3.12) was used for Figure 3.66. The fit is essentially the same for both cases. Therefore, the method involving alkanes was dropped in favor of the model for the alkenes (isobutylene), because the majority of the components in the product were alkene. The model involving CO inhibition was investigated because of the effect that CO/H_2 ratio had on conversion. The higher the CO partial pressure was (at same total pressure) the lower the conversion was for the same space time (Figure 3.30). Thus, it was possible that CO was inhibiting the reaction.

Figure 3.68 gives the best fit that could be obatined using Equation (3.16). The poor fit of the CO inhibition model led to its rejection and the acceptance of the model involving alkenes (n=4) as the major products with CO_2 inhibition. The final form used to determine parameters for all of the catalysts tested at more than one space time is given by Equation (3.27).

$$r_{CO} = \frac{k_p p_{CO} p_{H_2}^{0.5}}{\left(1 + K_{CO_2} p_{CO_2}\right)} \qquad (3.27)$$

Fitted parameters for isosynthesis catalysts

Table 3.26 shows the results of SimuSolv® modeling for all catalysts for which conversion data at more than one space time was available at 673 K, 50 atm, and 1/1 CO/H_2 ratio. When the rate constant is multiplied by the catalyst bulk density the agreement in rankings between model and experiment is excellent. Table 3.27 presents the parameters obtained at other reaction conditions. Figure 3.69 illustrates the agreement between predicted and experimental carbon monoxide conversions for the catalysts and conditions given in Tables 3.26 and 3.27.

For those catalysts tested at three temperatures it was possible to calculate an activation energy for the reaction and a heat of adsorption for carbon dioxide. These values were calculated in the traditional manner by plotting $\ln k_p$ (or $\ln K_{CO_2}$) versus $(1/T-1/T_o)$ where T_o is a reference temperature (usually taken as midpoint of temperature range of interest). Examples of these two plots are shown in Figures 3.70 and 3.71. The solid line represents the least-squares fit of the experimental points. The lowest temperature point for k_p was not used in determining the fit. As described in the earlier section on hydrogen sulfide experiments, the data used to determine the rate constant at this temperature were taken after temperature cycling had occurred. Thus, there was some deactivation and the fitted rate constant was lower than what would be expected. The CO_2 adsorption equilibrium constant was not affected by the deactivation.

Table 3.28 gives the results of the least squares fit for those catalysts tested at three or more temperatures. The numbers obtained from the fit are reasonable, though they are lower than those calculated by Maruya *et al.* (*10*) for C_2, C_3, and linear C_4 hydrocarbon formation. The lower activation energy for the cerium catalyst with the iron carbon monoxide cylinder suggests that diffusional limitations are more important in this case.

Equation Development for Modeling of the Product Distribution (Fixed Bed)

Extension of CO rate equation

The product distribution was modeled with a simple extension of the rate equation for predicting carbon monoxide conversion according to

$$\frac{dn_i}{dW} = r_i = \gamma_i r_{CO} = \gamma_i\left(-\frac{dn_{CO}}{dW}\right) \qquad i = 1,2,3,4,5+ \qquad (3.28)$$

which reduces to

$$\frac{df_i}{d\tau} = \gamma_i\left(\frac{dx}{d\tau}\right) \qquad f_i = \frac{n_i}{n_{CO}^o} \tag{3.29}$$

An expression for $dx/d\tau$ has already been found using SimuSolv®. Each of the γ_i's was found by using SimuSolv and the appropriate set of f_i's. A constraint on the γ_i's is found by writing a carbon balance for the reaction on which the rate equation for carbon monoxide conversion is based. This balance is given in the following equation.

$$r_{CO} = \sum r_i \alpha_{ci} + \sum r_{CO_{2i}} \tag{3.30}$$

The α_{ci} is the number of carbon atoms in the product for the *ith* reaction where i=1,2,3,4,5+ (for methane through C_5+ products). The summation term involving carbon dioxide term is the amount of CO_2 formed from the *ith* reaction. From the stoichiometry of the reaction it can be shown that

$$\sum r_{CO_{2i}} = \frac{1}{2} r_{CO} \tag{3.31}$$

When this equality and the assumed form for r_i are substituted into the carbon balance the result is

$$\sum \alpha_{ci}\gamma_i = \frac{1}{2} \tag{3.32}$$

This constraint was incorporated into the SimuSolv® program. Another approach to γ_i comes from the stoichiometry of the reaction

$$\frac{r_i}{\left(\frac{1}{2\alpha_{ci}}\right)} = r_{CO} \tag{3.33}$$

Now if r_i/r_{CO} is assumed to be constant (as before), a new gamma can be defined based on the number of carbon atoms in the product of the *ith* reaction.

$$\frac{r_i}{r_{CO}} = \frac{1}{2\alpha_{ci}}\gamma_{ci} = \gamma_i \tag{3.34}$$

When this relationship is substituted into Equation (3.32) it can be shown that

$$\sum \gamma_{ci} = 1 \tag{3.35}$$

The γ_{ci} can be taken as a measure of the efficiency of converting carbon monoxide into hydrocarbons with i carbon atoms.

Semi-empirical kinetic model

The distributions of products in Fischer-Tropsch synthesis follow an Anderson-Schulz-Flory scheme:

$$P_{n+1} = \alpha P_n \tag{3.36}$$

where α is the probability of propagation (27). Here, the similarities and differences between F-T synthesis and isosynthesis are presented, and a semi-empirical model is developed by adding an adjustable parameter to the F-T distribution to account for the contribution of condensation reactions to the chain growth.

The following assumptions are made in developing a kinetic model for the correlation of product distributions in isosynthesis.

1. Assume the intermediates on the surface are formed by chain reactions of intermediates on the surface, including initiation, propagation and termination, and assume pseudo-steady state and first order reactions for the intermediates.
2. Assume CO insertions and condensations are the two mechanisms for chain growth, and CO insertions occur on intermediates of any carbon number whereas condensation reactions occur only on C_2 intermediates with a methoxide. The following chain propagation is obtained:

Formation of C_2 intermediates

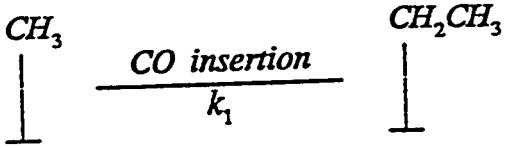

Formation of C_3 intermediates

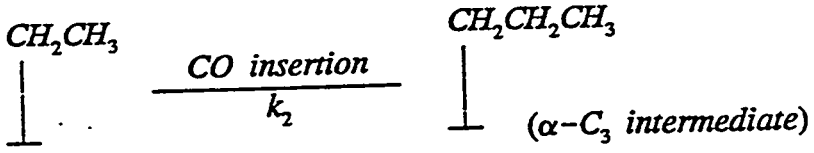

and

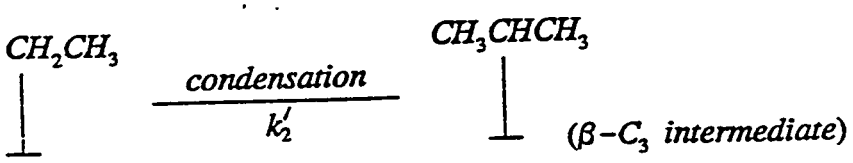

Formation of C_4 intermediates

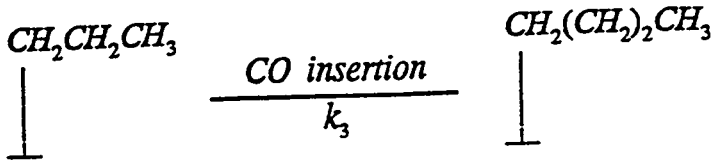

and

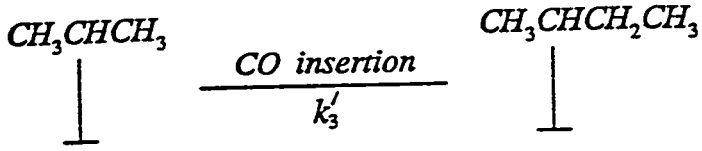

Formation of $C_{n>4}$ intermediates

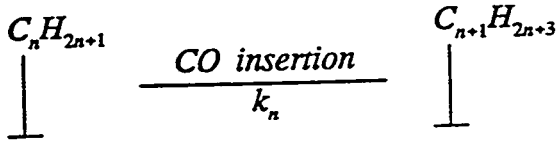

3. Assume that hydrocarbons are formed by the desorption of intermediates.

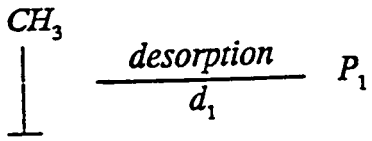

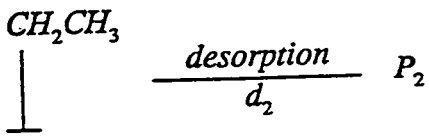

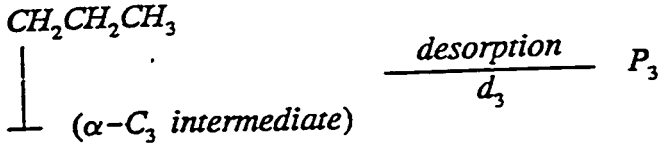

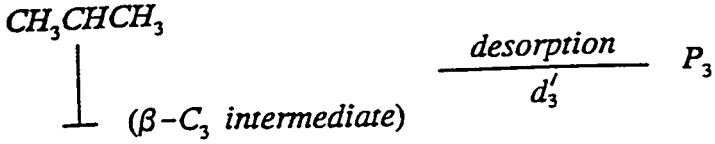

$$C_4H_9 \;\Big|\; \xrightarrow[d_4]{desorption} P_4$$

$$C_nH_{2n+1} \;\Big|\; \xrightarrow[d_n]{desorption} P_n$$

4. Assume the rate of desorption of β-C_3 intermediates is much slower than that of α-C_3 intermediates, i.e., $d_3' \ll d_3$. Assume all the intermediates other than β-C_3 intermediates satisfy the following relation:

$$\frac{k_i}{k_i + d_i} = \alpha \ (a\ constant). \tag{3.37}$$

The following product distributions are obtained:

$$\frac{P_2}{P_1} = \frac{\alpha}{1 + \alpha\kappa} \tag{3.38}$$

$$\frac{P_3}{P_2} = \alpha \tag{3.39}$$

$$\frac{P_4}{P_3} = \alpha + \kappa \tag{3.40}$$

$$\frac{P_{i+1}}{P_i} = \alpha \quad for\ i \geq 4 \tag{3.41}$$

where P_i is the mole fraction of hydrocarbons with carbon number i, and α and κ are defined as follows.

$$\alpha = \frac{k}{k + d}$$

$$\kappa = \frac{k_2'}{k_2} \tag{3.42}$$

The values of α and κ are obtained by fitting the experimental data to Equations (3.38) through (3.41).

After the distribution of hydrocarbon is correlated by the kinetic model, the production rate of hydrocarbons is further related with the reaction rate of CO by assuming that the reactions are represented as follows.

$$2nCO + \frac{m}{2}H_2 \rightarrow C_nH_m + nCO_2$$

From the stoichiometry, the production rate of hydrocarbons is given by the following.

$$r_{HC} = \frac{-r_{CO}}{\sum_{n=1}^{\infty} 2nP_n} \tag{3.43}$$

By combining with the empirical reaction rate of CO, the production rate of a C_n hydrocarbon is calculated using the following expression.

$$r_{C_n} = P_n r_{HC} = \frac{P_n}{\sum_{n=1}^{\infty} 2nP_n}(-r_{CO}) = \frac{P_n}{\sum_{n=1}^{\infty} 2nP_n} \frac{k_p p_{CO} p_{H_2}^{0.5}}{1+K_{CO_2} p_{CO_2}} \tag{3.44}$$

Results of Modeling of Product Distribution (Fixed Bed)

Extension of CO rate equation

Figure 3.72 shows the fit between experimental and predicted production rates for the C_1-C_5+ hydrocarbons for 7% Ce-ZrO_2. Table 3.29 contains the γ_i's and γ_{ci}'s obtained using SimuSolv® for each of three catalysts for which sufficient data at one temperature, pressure, and CO/H_2 ratio was available. For all three catalysts the fit is fairly good considering the simplicity of the model. For the 1.6% Na-ZrO_2 and 3.2% Ti, 2% Th, ZrO_2 catalysts the C_5+ fraction was slightly underpredicted. This may be the result of poor oxygenate analysis during these early runs. If oxygenates are lumped in with the C_5+ fraction then the constraint on the gammas is not exactly valid. The intercepts of the C_1-C_5+ production rates with zero space time are given by

$$\lim_{\tau \to 0}\left(\frac{dn_i}{dW}\right) = \lim_{\tau \to 0}\left(\gamma_i r_{CO}\right) \tag{3.45}$$

which can be reduced to

$$\lim_{\tau \to 0}\left(\frac{n_i}{W}\right) = \gamma_i k_p p_{CO}^{o} (p_{H_2}^{o})^{0.5} \tag{3.46}$$

The γ_{ci}'s in Table 3.29 show that the 7% Ce-ZrO_2 and 1.6% Na-ZrO_2 catalysts are more efficient at producing C_4's over methane in terms of carbon. The 1.6% Na-ZrO_2 seems to favor heavier hydrocarbons (possibly oxygenates included) over the C_1-C_4 fraction.

The 3.2% Ti, 2% Th, ZrO_2 catalyst is most efficient in producing methane.

Semi-empirical kinetic model

Figures 3.73 and 3.74 show that this semi-empirical model is capable of simulating the product distribution with two adjustable parameters. The values of α and κ vary with catalysts (Table 3.30). In general, an active isosynthesis catalyst has a large κ value and a catalyst that produces a large amount of heavy hydrocarbons has a large α value. The calculated production rate of C_n hydrocarbon generally agree well with the experimental values (Figure 3.75).

The semi-empirical kinetic model was developed by adding an adjustable parameter γ to the standard polymerization mechanism. This parameter is defined as the ratio of condensation to CO insertion. Several assumptions are made to develop the model, and they are discussed as follows.

The first and third assumptions are directly from the reaction mechanism. The steady state assumption seems to hold for isosynthesis since product distribution does not vary significantly with space velocity.

The second assumption states that condensations occur only between a methoxide and C^2 intermediates. This can be justified because steric hinderance may occur when the size of the intermediate increases.

The fourth assumption states that the rate of desorption of β-C_3 intermediates is much slower than that of α-C_3 intermediates, and hence, $k_3/d_3 \gg k_3'/d_3'$. Temperature programmed desorption was conducted to measure the activation energies of desorption for 2-propanol and 1-propanol on a precipitated zirconium oxide, and the values are about 35 and 20 kcal/mol, respectively. The large difference in the activation energies of desorption for 2-propanol and 1-propanol suggests that β-C_3 intermediates adsorbed much stronger than α-C_3 intermediates.

The semi-empirical model calculates the mole fractions of C_1, C_3 and C_4 quite accurately, but tends to underestimate the amount of C_5 hydrocarbons and overestimate C_2 (Figure 3.76). The error comes from the assumptions in the model. First, the reaction mechanism has been drastically simplified: condensations of intermediates other than C_2 are totally neglected and the interchanges between intermediates (such as a bond shift to form branched intermediates) are not taken into consideration. Second, the model completely neglects the desorption of β-C_3 intermediate, and assumes that α is a constant for all the other intermediates. Previous research on F-T synthesis has shown that the probability of propagation (equivalent to the parameter α in this study) might not be a constant for light hydrocarbons (*61*). Since mechanisms for branching were not included when deriving the kinetic model, the distributions of isomers were not calculated. This is a deficiency in the model.

Modeling of Slurry Reactors

To simulate isobutylene synthesis from synthesis gas performed in the slurry reactor in which decalin was used as the oil, it was assumed that there are only five reactions, which involve eight compounds, occurring during the synthesis process. These reactions are written as follows.

$$2CO + 2H_2 \rightarrow CH_4 + CO_2$$

$$2CO + H_2 \rightarrow \frac{1}{2}C_2H_4 + CO_2$$

$$2CO + H_2 \rightarrow \frac{1}{3}C_3H_6 + CO_2$$

$$2CO + H_2 \rightarrow \frac{1}{4}C_4H_8 + CO_2$$

$$2CO + H_2 \rightarrow \frac{1}{5}C_5H_{10} + CO_2$$

It was further assumed that (1) both the gas and liquid phases are perfectly mixed and (2) there is a dynamic equilibrium between the gas and liquid phases. Since the reactor was operated under constant temperature and pressure, only a mass balance is required. Based on the theory developed by Izarraraz *et al.* (62) for the vapor-liquid equilibrium involving chemical reactions, the following model equations were derived.

$$\sum_{i=1}^{N} \frac{z_i - \frac{\psi_i(\sigma_j)}{F}}{1 + \frac{V}{F}(K_i - 1) - \frac{1}{F}\sum_{i=1}^{N} \psi_i(\sigma_j)} - 1 = 0 \qquad (3.47)$$

$$\sigma_{CH_4} - r_{CH_4} W_{cat} = 0 \qquad (3.48)$$

$$\sigma_{C_2H_4} - 2r_{C_2H_4} W_{cat} = 0 \qquad (3.49)$$

$$\sigma_{C_3H_6} - 3r_{C_3H_6} W_{cat} = 0 \qquad (3.50)$$

$$\sigma_{C_4H_8} - 4r_{C_4H_8} W_{cat} = 0 \qquad (3.51)$$

$$\sigma_{C_5H_{10}} - 5r_{C_5H_{10}} W_{cat} = 0 \qquad (3.52)$$

where

i=H_2, CO, CO_2, CH_4, C_2H_4, C_3H_6, C_4H_8, C_5H_{10}, and decalin
j=CH_4, C_2H_4, C_3H_6, C_4H_8, and C_5H_{10}

The rate expression for compound j is the same as used for the fixed bed case:

$$r_j=\gamma_j r_{CO} \tag{3.53}$$

The symbols are defined in the notation section. It is noted that ψ_i is the amount of component *i* reacted or produced during the synthesis reactions, which are dictated by the following stoichiometric relationships.

$$\psi_{H_2} = 2\sigma_{CH_4} + \sigma_{C_2H_4} + \sigma_{C_3H_6} + \sigma_{C_4H_8} + \sigma_{C_5H_{10}} \tag{3.54}$$

$$\psi_{CO} = 2\left(\sigma_{CH_4} + \sigma_{C_2H_4} + \sigma_{C_3H_6} + \sigma_{C_4H_8} + \sigma_{C_5H_{10}}\right) \tag{3.55}$$

$$\psi_{CO_2} = -\left(\sigma_{CH_4} + \sigma_{C_2H_4} + \sigma_{C_3H_6} + \sigma_{C_4H_8} + \sigma_{C_5H_{10}}\right) \tag{3.56}$$

$$\psi_{CH_4} = -\sigma_{CH_4} \tag{3.57}$$

$$\psi_{C_2H_4} = -\frac{1}{2}\sigma_{C_2H_4} \tag{3.58}$$

$$\psi_{C_3H_6} = -\frac{1}{3}\sigma_{C_3H_6} \tag{3.59}$$

$$\psi_{C_4H_8} = -\frac{1}{4}\sigma_{C_4H_8} \tag{3.60}$$

$$\psi_{C_5H_{10}} = -\frac{1}{5}\sigma_{C_5H_{10}} \tag{3.61}$$

$$\psi_{decalin} = 0 \tag{3.62}$$

The last term in the denominator of Equation (3.47) is the summation of the contributions from the six reactions, and it is determined by Equation (3.63).

In the above model equations, there are a total of six unknowns, which are the vapor flow rate V and reaction extent σ_j, and six nonlinear equations. A computer code was developed in which a IMSL subroutine named NEQNF was utilized (uses a modified Powell

$$\sum_{i=1}^{N} \psi_i(\sigma_j) = 2\sigma_{CH_4} + \frac{3}{2}\sigma_{C_2H_4} + \frac{5}{3}\sigma_{C_3H_6} + \frac{7}{4}\sigma_{C_4H_8} + \frac{9}{5}\sigma_{C_5H_{10}} \quad (3.63)$$

hybrid algorithm and a finite difference approximation to the Jacobian) to solve the nonlinear equations.

The rate expression for CO was derived from the fixed bed experimental data.

$$r_{CO} = \frac{k_p p_{CO} p_{H_2}^{0.5}}{\left(1 + K_{CO_2} p_{CO_2}\right)} \quad (3.27)$$

Under the operating conditions, it could be further assumed that the gas phase is a perfect gas mixture and the liquid phase is an ideal solution.

The kinetic parameters for the two types of catalysts used in the slurry reactor are listed in Table 3.31.

The phase equilibrium constants K_i for CH_4, C_2H_4, and C_3H_6 were taken from Norris *et al.* (*63*). However, because of lack of information for C_4H_8 and C_5H_{10}, the corresponding K_i values of C_4H_{10} and C_5H_{12}, which were taken from the same reference, were used for C_4H_8 and C_5H_{10} in the modeling. The K_i values for H_2, CO, and CO_2 came from Graaf *et al.* (*64*). The values of K_i are summarized in Table 3.32.

The predicted product distributions at the CO/H_2 feed ratio of 1/1 are summarized in Tables 3.33 and 3.34 for the two different catalysts used, respectively.

It was noted for the model predictions that the feed ratios of hydrogen to carbon monoxide only affected the synthesis conversions but did not change the product distribution. The predicted conversions at different feed ratios are listed in Table 3.35.